Magnetized sawdust for removal of Cu (II) and Ni (II) from aqueous solutions

Meghna Kapur, Monoj Kumar Mondal*

Department of Chemical Engineering and Technology, Indian Institute of Technology (Banaras Hindu University), Varanasi 221005, Uttar Pradesh, India, Tel. +91 9452196638; Fax: +91 5422367098; emails: meghnakapur07@gmail.com (M. Kapur), mkmondal13@yahoo.com (M.K. Mondal)

ABSTRACT

An agricultural waste, sawdust was modified into magnetic nanoadsorbent (Fe_3O_4-SD) and used for single and bicomponent removal of Cu(II) and Ni(II) ions from aqueous solution. Adsorbent particles were characterized through XRD, TEM, FTIR, vibrating sample magnetometer, and Brunauer–Emmett–Teller analysis. The effect of initial metal concentration, contact time, adsorbent dose, pH, and temperature was studied within a suitable range. A contact time of 90 min was needed for equilibrium to be established. Adsorption of Cu(II) and Ni(II) ions onto Fe_3O_4-SD decreased with increase in temperature showing exothermicity. Process was found to be thermodynamically favorable and spontaneous and physical in nature. Equilibrium data fitted well with Langmuir isotherm model and followed pseudo-second-order kinetics. Adsorption capacity achieved was less when Cu(II) and Ni(II) coexisted in the solution in comparison with when they acted independently, thus supporting antagonistic behavior. Technical feasibility of Fe_3O_4-SD has been reported in the work and its easy fabrication and reusability make it a promising adsorbent.

Keywords: Adsorption; Cu(II) and Ni(II); Fe_3O_4-SD; Isotherms; Regeneration

1. Introduction

Rapid implementation of nanomaterials has already started. They have entered to the lives through different fields. Nanomaterials are getting utilized in medical area for magnetic resonance imaging and drug delivery system [1]. Magnetic nanoparticles are used in diagnostics and molecular biology [2]. Silver nanomaterials are extensively used in appliances [3] and in crockery fabrication as they possess antibacterial properties [4]. Due to antifouling properties of TiO_2, it is used as a glaze guard. Other applications include formation of paints and catalysts [5], fireproof glass, and for UV protection [6]. Magnetic nanoparticles due to its magnetic behavior have shown new approaches. In context to the water treatment, magnetic as well as non-magnetic nanoparticles have proved to be quite efficient owing to the high surface area. For treating the heavy metal containing solutions, manganese oxide nanomaterial [7], nanoporous titania adsorbents [8], magnetic hydroxyapatite nanoparticles [9], nanoalumina [10], and magnetic nanoparticle (Fe_3O_4) impregnated onto tea waste [11] have been extensively used by many researchers.

Earlier, the low-cost agricultural wastes or industrial byproducts have shown promising results in the

*Corresponding author.

removal of even low concentration of metallic species viz. rice husk [12], bagasse and fly ash [13], stem waste [14], fruit peels [15], fly ash [16], and blast furnace slag [17]. The approach of this work is to transform an agricultural waste into magnetic nanoparticles so as to improve its adsorptive capacity. Agricultural waste chosen for this is *Mangifera indica* sawdust and the magnetic behavior of the particle formed is quite useful in phase (solid–liquid) separation. Sawdust has cellulosic nature, composed of bonded –OH groups, C–O stretching in alcohols, symmetrical –NO groups present at the surface for binding [18]. Sawdust is a valuable agricultural waste having potential of adsorbing ions from aqueous solutions, but it was not effective in adsorbing two ions simultaneously from aqueous solutions. On the basis of the study done by many researchers, some chemical treatments on sawdust were tested. Modifications through citric acid, phosphoric acid [19], and sodium sulfide [20] have been proved suitable for adsorbing cations earlier, but no such treatment suited adsorption of the two metals simultaneously from the solution. Finally, the properties of the sawdust were further enhanced by making into magnetic nanoparticle and providing them with much larger surface area, thus improving its application as adsorbent for not only single metal containing solutions but also for combined Cu(II) and Ni(II) system.

Present work has been focused on simultaneous removal of Cu(II) and Ni(II) from aqueous solutions using magnetic nanoparticles of *M. indica* sawdust (Fe$_3$O$_4$-SD). These Cu(II) and Ni(II) ions are in general present in the effluent of electroplating industries. Primarily, the aim of the study is to (a) synthesize a novel magnetic nanomaterial by co-precipitation method using naturally obtained sawdust; (b) confirmation of its structural and surface properties through XRD, TEM, FTIR, vibrating sample magnetometer (VSM), and Brunauer–Emmett–Teller (BET) analysis; (c) batch adsorption studies by varying pH, time of contact, agitation speed, temperature, initial Cu(II) and Ni(II) concentration, and temperature; (d) kinetics model investigation; (e) isotherms and interference studies in the multicomponent system; and (f) reusability studies of the adsorbent.

2. Experimental

2.1. Reagents

All the reagents used were of analytical grades. Cupric nitrate [Cu(NO$_3$)$_2$·3H$_2$O] and ammonium nickel(II) sulfate [(NH$_4$)$_2$SO$_4$NiSO$_4$·6H$_2$O] were dissolved in double-distilled water to prepare

1,000 mg/L of stock solution of Cu(II) and Ni(II) ions, respectively. All the working solutions were prepared by diluting the stock solutions using double-distilled water. Additional chemicals which were required for adsorbent preparation are ferric chloride hexahydrate, ferrous sulfate heptahydrate, ammonia solution, sodium hydroxide, and hydrochloric acid.

2.2. Adsorbent preparation

For synthesizing Fe$_3$O$_4$-SD at first, *M. indica* sawdust collected from a local sawmill was thoroughly washed with double-distilled water to make it dust free and then sieved. It was then dried in an oven at 50°C for 24 h. For the impregnation of sawdust with magnetic properties in a nanorange, co-precipitation of FeCl$_3$·6H$_2$O and FeSO$_4$·7H$_2$O along with sieved sawdust particles was done [21]. Exactly, 6.1 g of FeCl$_3$·6H$_2$O and 4.2 g of FeSO$_4$·7H$_2$O in 100 mL of distilled water were heated to 90°C and then 10 mL of ammonium hydroxide and 1 g of sieved sawdust (average particle size—96.5 μm) dissolved in 200 mL of distilled water was added to it. The pH of the medium was adjusted to 10 and again heated to 80°C, and then cooled for precipitate formation. Black precipitate formed was filtered, dried overnight, and stored in a desiccator.

2.3. Analytical methods

For the characterization of the adsorbent used in the present study, X-ray diffraction analysis was done using Philips 1710 X-ray diffractometer employing nickel-filtered Cu Kα target of radiation wavelength 1.542 Å operating at 40 kV and 40 mA. Through the patterns obtained in XRD analysis, phase confirmation of the adsorbent can be done and it also helps in determining the size range of the particles. Morphology and dimensions of the nanomaterial formed were determined by transmission electron microscopy (Tecnai G^2 series 200 kV TEM). Parameters such as BET surface area, pore area, and pore volume were determined by N$_2$ adsorption–desorption method using Micromeritics ASAP 2020, V302G single port. Nitrogen was used as the cold bath (77 K) and BET theory was used. For porous structures, BJH (Barrett–Joyner–Halenda) data were used. To examine the magnetic properties, the nanoparticles were studied by a VSM at room temperature. The plots of magnetization vs. magnetic field (*M–H* loop) at 28.6°C were obtained. Magnetic measurement was carried out on a quantum design MPMS-XL5 SQUID magnetometer using 0.02684-g sample. The pH

measurements were done using digital pH meter (Systronics). Meter was standardized using buffer solutions of pH 4.0, 7.0, and 9.2. For shaking the adsorbent–adsorbate system at a constant temperature, water bath shaker (NSW-133) was used for all the adsorption experiments. Magnetic stirrer with hot plate was used for heating the solution and providing the required temperature for precipitate formation. Analysis of Cu(II) and Ni(II) concentration in the solution was carried out using UV–visible spectrophotometer (ELICO SL 159 UV–vis Spectrum).

2.4. Adsorption equilibrium experiments

Batch adsorption of Cu(II) and Ni(II) was investigated onto Fe_3O_4-SD nanoparticle formed out of sawdust. Experiments were carried out at various operating conditions. The Cu(II) or Ni(II) concentration in the binary solution ranged between 5 and 100 mg/L. Variation of working parameters viz. pH (2–7), adsorbent dose (1–6 g/L), time of contact (0–120 min), agitation speed (0–200 rpm), and temperature (20–40°C). Kinetic experiments were done for a solution containing 100 mg/L of each Cu(II) and Ni(II) at (30 ± 1)°C at least twice and mean values were used in the analysis and plotting of the data. Isotherm studies for single and bicomponent solutions were done in the range of 50–150 mg/L.

Adsorbents were filtered after the equilibrium was achieved and the Cu(II) and Ni(II) concentration in the filtrate was analyzed by forming colored complexes for both Cu(II) and Ni(II) using UV–visible spectrophotometer. Cu(II) gave yellow color with dimethyldithiocarbamate and was tested at 457 nm, while a red unstable complex was observed for Ni(II) with dimethylglyoxime and it was read at 445 nm [22]. The adsorbed amount of ions onto Fe_3O_4-SD nanoparticle at each interval of time is calculated by following equation:

$$\% \text{ Removal of metal ions} = \frac{C_o - C_f}{C_o} \times 100 \qquad (1)$$

Quantity of Cu(II) and Ni(II) ions adsorbed per unit mass of adsorbent is given by

$$q = \frac{(C_o - C_e)V}{W} \qquad (2)$$

All the investigations were carried out in duplicate to avoid any discrepancy in experimental results with the reproducibility and the relative deviation of the order of ±0.5 and ±1.5%, respectively, for the two ions (Cu(II) and Ni(II)).

2.5. Reusability of adsorbent

To test the reusability of adsorbent, Cu(II)- and Ni(II)-loaded Fe_3O_4-SD nanoparticles were washed with different eluents. Distilled water, dilute solutions of HCl, HNO_3, and H_2SO_4 were tested for regenerating the adsorbent. 100 mL of aqueous solution containing 10 mg/L of each Cu(II) or Ni(II) ion and adsorbent dose of 5 g/L was given constant shaking of 120 rpm at 30 ± 1°C. The adsorbent was then separated from the solution and dipped in 0.1 N HCl, 0.1 N HNO_3, 0.1 N H_2SO_4, and distilled water and was again constantly agitated at 120 rpm. The concentration of Cu(II) and Ni(II) ions released into the eluent was tested and the suitable desorbing agent was selected. Consecutive adsorption–desorption cycles were run using the eluent with the highest desorbing power and the validation of reusability of the Fe_3O_4-SD nanoparticles for bicomponent adsorption was set.

Desorption efficiency of the eluents can be calculated using the following equation:

$$\text{Desorption efficiency} = \frac{\text{Concentration of metal desorbed}}{\text{Concentration of metal loaded}} \times 100$$

$$(3)$$

3. Results and discussion

3.1. Characterization of Fe_3O_4-SD

The XRD demonstrates high crystallinity of Fe_3O_4-SD nanoparticles. Phase of Fe_3O_4 is revealed from the patterns of the XRD obtained. Major peaks of Fe_3O_4-SD were visualized at 30.1°, 35.5°, 43.1°, 53.4°, 57.0°, and 62.6° with their respective indices (2 2 0), (3 1 1), (4 0 0), (4 2 2), (5 1 1), and (4 4 0) as shown in Fig. 1(a). In consistency with the database in JCPDS file (PCPDFWIN v.2.02, PDFNo. 85-1436), it showed pure Fe_3O_4 with inverse-spinel structure and sawdust binding did not result in phase change [21].

The crystallite size of the particle was estimated using Debye–Scherrer equation [23]:

$$X_s = \frac{0.9\lambda}{(\text{fwhm}) \cos \theta} \qquad (4)$$

where X_s is the crystallite size (nm), λ is the X-ray wavelength (0.15406 nm), and fwhm is the full width at half maximum for the diffraction peak, and θ is the
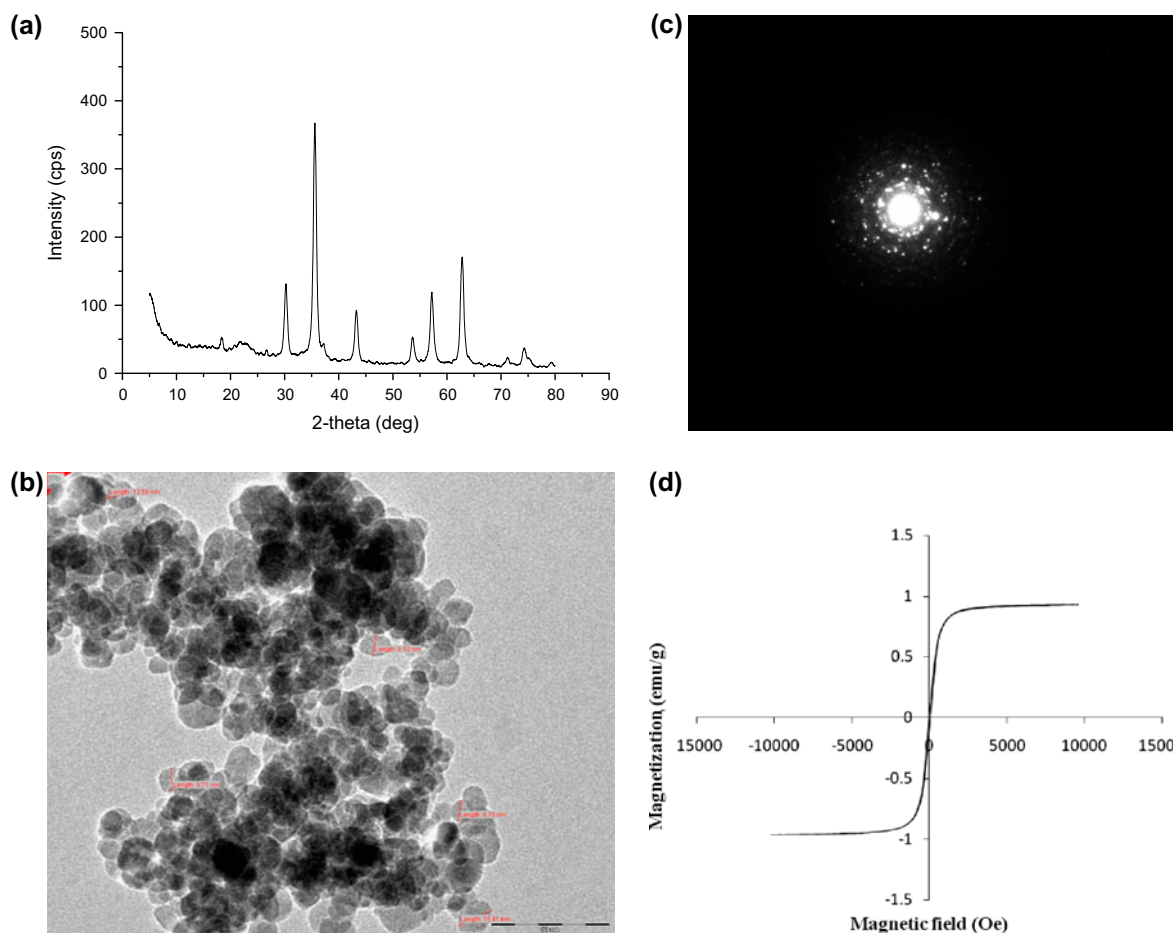
(a)

(c)

(b)

(d)

Fig. 1. Characterization of Fe_3O_4-SD nanoparticles (a) XRD plot, (b) TEM image, (c) diffraction pattern, and (d) magnetization curves.

diffraction angle. Average crystallite size obtained was 30 nm.

The picture of TEM in Fig. 1(b) reveals smaller and compact particles in a nanorange with particle diameter of 50 nm. Diffraction pattern of the particle is also shown in Fig. 1(c). The BET surface area obtained was 41.7414 m^2/g, whereas BJH adsorption/desorption surface area of pores is 34.091/42.2112 m^2/g. The single-point total pore volume of pores (d < 21.960 Å) was found to be 0.019624 cm^3/g, whereas cumulative adsorption/desorption pore volume of the pores (17 Å < d < 3,000 Å) is 0.063438/0.072568 cm^3/g, respectively. The average pore diameter by BET method was found to be 18.8050 Å, whereas the BJH adsorption/desorption average pore diameter is 74.435/68.766 Å. Fe_3O_4-SD was found to comprise mainly of mesopores (87% from BJH adsorption and 99.5% BJH desorption).

It was analyzed from the FTIR spectra (before adsorption) of Fe_3O_4-SD nanoparticles that it exhibits

strong bands of iron oxide in the low frequency region (1,000–400 cm^{-1}) due to the iron oxide skeleton [24]. The spectrum is consistent with magnetite Fe_3O_4 spectrum (bands at 629.6, 584.1, and 428.9 cm^{-1}). This supports complete association of sawdust with magnetic Fe_3O_4 particles. Bands after adsorption shifted to 581.7 and 407 cm^{-1}, while peak at 629.6 disappeared. Spectroscopic bands at 3,453.1 cm^{-1} represent bonded –OH groups [11] which then dropped to 3,180.5 cm^{-1}. At 1,321.2 cm^{-1}, bands of NO^{2-} bonded through nitrogen were observed [25]. Peak at 1,635.1 cm^{-1} was observed representing C=O stretching of carboxylate [26]. Shifts were seen to 1,335.5 and 1,656.4 cm^{-1} which signifies NO^{2-} bonding and C=O stretching vibrations are involved in Cu(II) and Ni(II) binding. Appearance of a new peak was noticed after adsorption of the Cu(II) and Ni(II) ions at 1,156.5 cm^{-1} signifying C–O–C stretch in ether [21]. Also, the Fe–O bonds and –OH are possibly involved in the activity.

Magnetization curve of the Fe$_3$O$_4$-SD exhibits near-zero coercivity and remanence suggesting super paramagnetic nature of the adsorbent [27]. From the plots of magnetization vs. magnetic field (Fig. 1(d)), the saturation magnetization strength (M_s) is 0.95 emu/g. The value is much lower which may be due to the nanosize effect [28]. It is known that the energy of a magnetic particle in an external field is proportional to its size via the number of magnetic molecules in a single magnetic domain and as this energy becomes comparable to the thermal energy, thermal fluctuations significantly reduce the total magnetic moment at a given field [29].

3.2. Effect of pH

The effect of pH on adsorption of Cu(II) and Ni(II) ions was investigated in both acidic and alkaline range. Adsorption was studied at room temperature for pH variation of 2–8 (Fig. 2). Removal percentage for Cu(II) was seen increasing from 20 to 99.27 and 50 to 98.63 for Ni(II) in the pH range 2–5 and again it dropped down for pH 6–8. Maximum adsorption efficiency was noted at pH 5 which was 99.27 and 98.63% for Cu(II) and Ni(II), respectively. Cu(II) can be present in the aqueous solution as Cu^{2+}, $Cu(OH)^+$, $Cu(OH)_2$, $Cu(OH)_3^-$, and $Cu(OH)_4^{2-}$. But the dominance of Cu^{2+} is seen at pH < 6 [30,31].

Similarly for Ni(II), Ni^{2+} ions are only present at pH <7, while Ni(II) can also be available as $Ni(OH)^+$, $Ni(OH)_2$, and $Ni(OH)_3^-$ in the aqueous solutions. To work on a binary solution, it is importan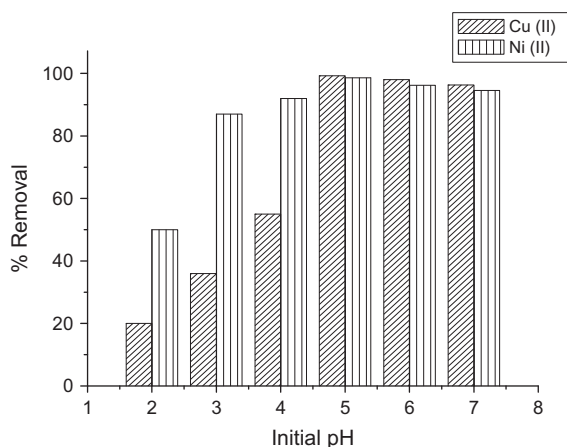t to choose pH <6, which su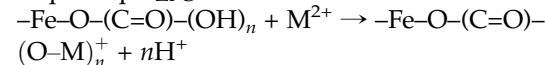its adsorption of both Cu(II) and Ni(II) ions. The pH chosen for the present study through experiments is 5, which is also strongly supported by the speciation diagram for copper and nickel.

The experimental results obtained can be explained by the surface charge and the pH$_{ZPC}$ of the adsorbent. At pH < pH$_{ZPC}$ (pH$_{ZPC}$ of Fe$_3$O$_4$-SD is 3.8), the adsorbent surface gets protonated and thus there exists a competition between H$^+$ and heavy metal ions (Cu^{2+} and Ni^{2+}) for the active sites making it unfavorable for metal binding. But as the pH is raised at a value greater than pH$_{ZPC}$, the adsorbent gets deprotonated and can bind Cu(II) and Ni(II) ions through electrostatic attraction leading to the formation of Cu(II) and Ni(II)—ligand magnetic composite complexes [21]. The main mechanism (complexation and ion exchange) of adsorption can be explained as

At pH < pH$_{ZPC}$:
$$-Fe-O-(C=O)-(OH)_n + H^+ \rightarrow Fe-O-(C=O)-(OH_2)_n^+$$
At pH > pH$_{ZPC}$:
$$-Fe-O-(C=O)-(OH)_n + M^{2+} \rightarrow -Fe-O-(C=O)-(O-M)_n^+ + nH^+$$

where M = Cu and Ni.

3.3. Effect of equilibration time and initial Cu(II) and Ni(II) concentration

The feasibility of Fe$_3$O$_4$-SD as a magnetic nanoadsorbent was tested for the removal of Cu(II) and Ni(II) ions from aqueous solutions. The solution of different concentrations varying between 10 and 100 mg/L

Fig. 2. Effect of initial pH on Cu(II) and Ni(II) removal by Fe$_3$O$_4$-SD nanoparticles (temperature: 30℃; pH: 5; adsorbent dose: 5 g/L; heavy metal concentration: 10 mg/L; and time: 90 min).
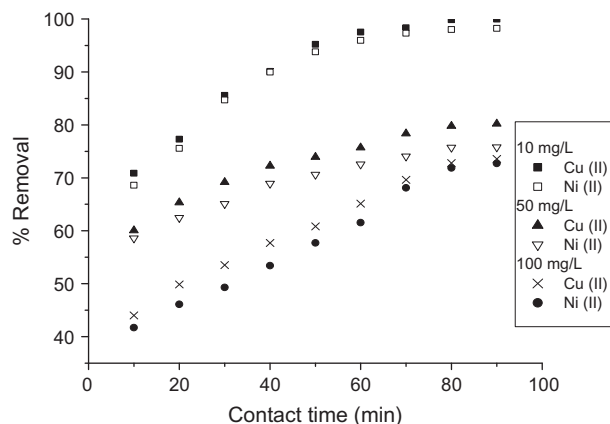

Fig. 3. Effect of contact time and initial Cu(II) and Ni(II) concentration on Cu(II) and Ni(II) removal by Fe$_3$O$_4$-SD nanoparticles (temperature: 30℃; pH: 5; adsorbent dose: 5 g/L; time: 90 min; and concentration: 10–100 mg/L).

containing both Cu(II) and Ni(II) species was shaken at constant temperature for a fixed dose of 5 g/L and sampling was done at regular intervals of 10 min. The filtrate was analyzed for Cu(II) and Ni(II) and the results are presented in Fig. 3. As predicted, the removal percentage for both species increased with time upto 90 min and then approached a constant value. On increasing concentration from 10 to 100 mg/L, the percentage removal for Cu(II) decreased from 99.98 to 73.58. Same trend was seen for Ni(II) ions for which percentage removal decreased from 98.22 to 72.71. In the initial stage, due to the large concentration gradient and the presence of vacant sites, adsorption was rapid while after attaining equilibrium, it dropped as a repulsive force appears between the metallic species in the solution and the sites already occupied by the same species. Adsorption noticeably decreased on increasing Cu(II) and Ni(II) concentration. High removal at low concentration is of industrial importance.

3.4. Effect of adsorbent dose

In comparison to other adsorbents, nanoadsorbents have higher surface area to volume ratio. Thus, for the present case, it is expected that high efficiency is achieved for a less amount of Fe$_3$O$_4$-SD. Effect of different adsorbent doses on removal of Cu(II) and Ni(II) ions has been observed. For this, dose was varied from 1 to 5 g/L and the Cu(II) and Ni(II) concentration, temperature, and pH were kept constant at 10 mg/L, 30 ± 1℃, and 5, respectively. Hundred percent adsorption was seen for Cu(II) ions at 3 g/L dose, while for Ni(II), it was achieved for a dose of 5 g/L. To select a common dose for 100% adsorption of both the ions from bicomponent system, a dose of 5 g/L was fixed. For a nanomaterial, greater availability of sites is the reason behind such high adsorptive power.

3.5. Effect of agitation speed

Agitation effect on adsorption of Cu(II) and Ni(II) was investigated within a range of 0–120 rpm. Adsorption was quite low at no agitation and rapidly increased with agitation speed. Adsorption percentage achieved at no shaking for Cu(II) was 18 and for Ni(II) ions, it was 20 which increased up to 99.27 and 98.63, respectively, for Cu(II) and Ni(II) at 120 rpm. Probably, at lower speeds, adsorbing particles agglomerate and whole of the surface is not available for adsorbing the Cu(II) and Ni(II) species, while at higher speeds, the particles get dispersed and participate in the process.

3.6. Effect of temperature

Temperature has an important role to play behind adsorption. Equilibrium adsorption capacity is affected by the change in temperature. For exothermic reaction, adsorption capacity decreases with increase in temperature and the reverse is true for endothermic reactions. Temperature effect was investigated for a solution containing 100 mg/L of both Cu(II) and Ni(II) ions at pH 5 for the temperature range 20–40℃. Fig. 4 shows the removal percentage of solution at different temperatures with respect to time. For both the species, adsorption was seen decreasing with increase in temperature, indicating exothermic reaction. Increasing temperature was not favorable for the simultaneous removal of both Cu(II) and Ni(II). On increasing temperature, the randomness of the system increases, thus the probability of ions being captured by the Fe$_3$O$_4$-SD surface decreases.

3.7. Kinetic studies

Solute uptake rate is described by the kinetics. Rate-determining step can be established which thus helps in designing the process. Experiments were carried out for 100 mg/L of solution containing Cu(II) and Ni(II) ions in the same ratio. Kinetics was tested using pseudo-first-order kinetics, second-order rate kinetics, Elovich, and intraparticle diffusion model.

3.7.1. Pseudo-first-order kinetics

The linearized form of the pseudo-first-order kinetics model as proposed by Lagergren [32] is:
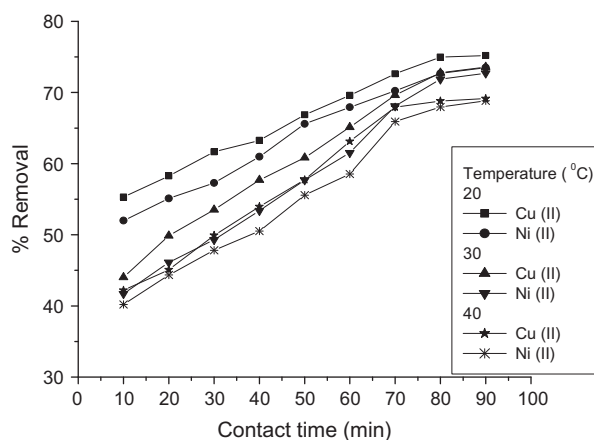

Fig. 4. Effect of temperature on Cu(II) and Ni(II) removal by Fe$_3$O$_4$-SD nanoparticles (pH: 5; adsorbent dose: 5 g/L; heavy metal concentration: 100 mg/L; and time: 90 min).

$$\log (q_e - q_t) = \log \ q_e - \frac{(k_1)t}{2.303} \qquad (5)$$

where q_e and q_t are the amounts of Cu(II) and Ni(II) adsorbed (mg/g) at equilibrium time and at any time t, respectively; k_1 (min^{-1}) is the first-order rate constant.

3.7.2. Pseudo-second-order kinetics

Pseudo-second-order [33] is described by the following equation:

$$\frac{t}{q_t} = \frac{1}{k_2 q_e^2} + \frac{t}{q_e} \qquad (6)$$

where k_2 (g/mg min) is the second-order rate constant.

3.7.3. Elovich kinetics

Elovich equation is generally applied for chemisorption. It is devised for heterogeneous surfaces [34] and stated as:

$$q_t = \frac{1}{\beta} \ \ln(\alpha\beta) + \frac{1}{\beta} \ \ln(t) \qquad (7)$$

$$q_t = A + B \ \ln \ t \qquad (8)$$

where α and β are the Elovich constants. α (mg/g min) represents the rate of chemisorptions at zero coverage, and β (g/mg) is related to the extent of surface coverage and activation energy for chemisorptions.

3.7.4. Intraparticle diffusion

Weber and Morris [35] devised a model for intraparticle diffusion as:

$$q_t = K_{id} t^{1/2} \qquad (9)$$

where K_{id} (mg/g min$^{1/2}$) represents the intraparticle diffusion rate constant. Pseudo-first-order kinetics model was tested for a set of temperatures ranging from 20 to 40°C in a binary solute system. From the plot of $\log(q_e - q_t)$ vs. t, quantity of Cu(II) and Ni(II) adsorbed and the rate constants obtained at the respective temperatures are given in Table 1. R^2 showed a much lesser value for the kinetics of Cu(II) as well as Ni(II) ions.

For the present study, pseudo-second-order model was found to be the most suitable. Parameters (Table 1) were obtained through a plot of (t/q_t) vs. t. Values of the correlation coefficient were seen to be 0.993 and 0.994 for Cu(II) and between 0.986 and 0.988 for Ni(II)

Table 1
Kinetic and thermodynamic parameters for adsorption of Cu(II) and Ni(II) using Fe$_3$O$_4$-SD nanoparticles

Species Temperature (°C)		Copper(II)			Nickel(II)		
		20	30	40	20	30	40
Pseudo-first-order kinetics	q_e (mg/g)	6.47	5.28	4.40	5.649	5.727	5.997
	k_1(min^{-1})	0.025	0.018	0.018	0.013	0.013	0.020
	R^2	0.878	0.860	0.843	0.860	0.867	0.865
Pseudo-second-order kinetics	q_e	15.38	14.28	13.51	13.69	13.69	13.69
	k_2(g/mg min)	0.009	0.012	0.015	0.011	0.010	0.009
	R^2	0.993	0.993	0.994	0.988	0.987	0.986
Elovich model	A	6.431	6.555	7.218	5.82	5.66	5.19
	B	1.774	1.604	1.301	1.637	1.638	1.683
	R^2	0.901	0.843	0.813	0.713	0.701	0.801
Intraparticle diffusion	K_{id} (mg/g min$^{1/2}$)	0.625	0.569	0.465	0.598	0.602	0.608
	R^2	0.972	0.919	0.903	0.826	0.822	0.906
$\Delta G°$ (kJ/mol)		−2.7	−2.56	−2.09	−2.48	−2.46	−2.06
$\Delta H°$ (kJ/mol)		−1.14			−8.60		
$\Delta S°$ (kJ/mol K)		−0.029			−0.02		

ions of the binary system. Elovich model dealing with chemisorption kinetics was analyzed by graph between q_t and $\ln(t)$. Constants obtained along with the R^2 values are listed which show poor fit of the data. For intraparticle diffusion to be the controlling mechanism, a plot of q_t against square root of contact time should result in a straight line passing through origin; otherwise, film diffusion plays an important role. It was inferred that the plot does not pass through the origin implying the role of film diffusion and only the intraparticle diffusion. Thus, second-order kinetics appropriately suits the kinetics of both Cu(II) and Ni(II) ions of the binary solution. Combined film and intraparticle diffusion has also a role to play.

3.8. Thermodynamic studies

Studies relevant to the effect of temperature on simultaneous adsorption of Cu(II) and Ni(II) ions onto Fe_3O_4-SD not only decide the nature of the process (endothermic or exothermic) but also help in understanding the thermodynamic states. Change in standard free energy ($\Delta G°$) is obtained using the following equations:

$$K_c = C_{Ae}/C_e \qquad (10)$$

$$\Delta G° = -RT \ \ln K_c \qquad (11)$$

Values of enthalpy ($\Delta H°$) and entropy ($\Delta S°$) can be calculated through the plot of $\ln K_c$ vs. $1/T$ by

$$\ln \ K_c = (\Delta S°/R) - (\Delta H°/RT) \qquad (12)$$

where K_c is the equilibrium constant at temperature T, R is the universal gas constant (8.314×10^{-3} kJ/mol K), and C_{Ae} and C_e are the equilibrium concentrations of adsorbate on the adsorbent and in the solution, respectively.

As it can be seen from the parametric values given in Table 1, the negative value of $\Delta G°$ indicates spontaneity and favorable adsorption. Moreover, the adsorption is physical in nature as $\Delta G°$ lies between −20 and 0 kJ/mol and not between −80 and −400 kJ/mol which signifies chemisorption. The negative values of $\Delta S°$ and $\Delta H°$ support exothermicity and low degrees of freedom. Also, $\Delta H° < 40$ kJ/mol indicates physical adsorption [36].

3.9. Adsorption isotherms and statistical analysis

Equilibrium data or the adsorption isotherms establish a relationship between the amount of adsorbate per unit of adsorbent (q_e) and its equilibrium solution concentration (C_e) at constant temperature. Affinity of an adsorbent in the form of adsorption capacity can be modeled using Langmuir, Freundlich, and Redlich–Peterson isotherms. For this, experiments have been performed over a range of initial Cu(II) and Ni(II) concentrations of 50–150 mg/L containing Cu(II) and Ni(II) ions at pH 5.

Langmuir model assumes monomolecular layer adsorption at homogeneous sites. Linear form for which can be expressed as:

$$\frac{C_e}{q_e} = \frac{1}{q_o b} + \frac{C_e}{q_o} \qquad (13)$$

where q_e is the amount adsorbed per unit mass of adsorbent at equilibrium (mg/g) and C_e is the equilibrium concentration (mg/L). The Langmuir constants related to the adsorption capacity and energy of adsorption are denoted by q_o and b, respectively.

Freundlich model for heterogeneous surfaces is defined as:

$$\ln \ q_e = \ln \ K_F + \frac{1}{n} \ \ln \ C_e \qquad (14)$$

K_F and n related to adsorption capacity and intensity, respectively.

Redlich–Peterson is an improvement over Langmuir and Freundlich model and is described as:

$$\ln \left(K_R \frac{C_e}{q_e} - 1 \right) = \ln \ a_R + \beta \ \ln \ C_e \qquad (15)$$

where C_e is the equilibrium concentration (mg/L), K_R (g^{-1}) and a_R (mg^{-1}) are the R–P isotherm constants, and β is the exponent ($0 < \beta < 1$). Experimental and predicted values have been quantified statistically using regression coefficient (R) and correlation coefficient (R^2) and error analysis using Chi-square (χ^2) and root mean square error (RMSE) for all sets of isotherms.

Chi-square test

Chi-square test computed by the following equation:

$$\chi^2 = \sum \frac{(q_{e,exp} - q_{e,model})^2}{q_{e,model}} \qquad (16)$$

Root mean square error (RMSE)

RMSE is defined as follows:

$$\text{RMSE} = \sum \left(\frac{q_{e,\text{exp}} - q_{e,\text{model}}}{q_{e,\text{model}}} \right)^2 \qquad (17)$$

3.9.1. Monocomponent adsorption

Analysis of the equilibrium adsorption data for solution in the range of 50–150 mg/L containing either Cu(II) or Ni(II) ions was done for understanding monocomponent system. Data were fitted to Langmuir, Freundlich, and Redlich–Peterson models. The parameters obtained through Langmuir, Freundlich, and Redlich–Peterson isotherms for each metal ion

were given in Table 2. The loading capacity for Cu(II) was 23.8 and 19.2 mg/g for Ni(II) as obtained through Langmuir model. Statistical analysis (R and R^2) and error analysis (χ^2 and RMSE) are also presented in Table 3 which strongly supports the applicability of Langmuir and R–P model. Moreover, in case of R–P model, the value of β lies between 0 and 1 favoring the adsorption. Parameter for a single-solute system shows that Cu(II) has more affinity of getting adsorbed on the Fe_3O_4-SD nanoparticles.

3.9.2. Bicomponent adsorption

An interaction effect of Cu(II) and Ni(II) was studied in a bicomponent system. Cu(II) and Ni(II) ions, in the ratio, 1:1 were made in the range of 50–150 mg/L.

Table 2
Isotherm constants for monocomponent adsorption on Fe_3O_4-SD nanoparticles

Adsorbate	Langmuir constants		Freundlich constants		Redlich–Peterson constants		
	b (mg^{-1})	q_o (mg/g)	K_F	n	K_R (g^{-1})	a_R (mg^{-1})	β
Copper(II)	0.075	23.8	4.11	2.54	2	0.129	0.894
Nickel(II)	0.132	19.2	5.49	3.49	5	0.528	0.836

Table 3
Comparison of the experimental and calculated q_e values evaluated from the monocomponent isotherm models

C_o (mg/L)	C_e (mg/L)	$q_{e,\text{exp}}$ (mg/g)	$q_{e,\text{calc}}$ (mg/g)		
			Langmuir	Freundlich	R–P
Copper(II)					
50	7.22	8.55	8.39	8.94	8.21
75	14.16	12.16	12.28	11.64	11.86
100	24.09	15.18	15.34	14.35	14.91
125	39.1	17.18	17.77	17.36	17.61
150	54.22	19.15	19.12	19.74	19.34
R			0.999	0.990	0.998
R^2			0.998	0.980	0.997
χ^2			0.025	0.107	0.039
RMSE			0.001	0.008	0.003
Nickel(II)					
50	5.97	8.80	8.38	8.9	8.52
75	14.28	12.14	12.48	12.15	11.86
100	26.86	14.6	14.92	14.49	15.12
125	41.83	16.63	16.21	16.12	16.81
150	64.98	17.0	17.16	17.75	17.95
R			0.998	0.983	0.998
R^2			0.998	0.967	0.998
χ^2			0.047	0.017	0.05
RMSE			0.004	0.012	0.003

Table 4
Langmuir isotherm constants for single and multicomponent adsorption of Cu(II) and Ni(II) on Fe_3O_4-SD nanoparticles

Heavy metal ions	System	Langmuir constants			
		q_o (mg/g)	b (mg^{-1})	R^2	q^{mix}/q_o
Cu(II)	Cu(II) alone	23.8	0.075	0.998	
Ni(II)	Ni(II) alone	19.2	0.132	0.998	
Cu(II)	Cu(II) + Ni(II) (1:1)	20.0	0.065	0.981	0.840
Ni(II)		18.2	0.082	0.979	0.946

The ideal adsorbed solution theory [37] was developed to predict equilibria in dilute multicomponent liquid adsorption system; multicomponent adsorption isotherms could be predicted using single component data. Adsorption capacities as calculated from Langmuir isotherm model for the single Cu(II) or Ni(II) and binary mixtures (Cu(II) and Ni(II)) are given in Table 4. Ionic interaction can be judged by the ratio of adsorption capacity for a metal ion present with other ion (q^{mix}) to the adsorption capacity when present alone (q_o) in the aqueous system.

When $\frac{q^{mix}}{q_o} > 1$, the adsorption capacity is seen increasing due to the presence of other metal ions or shows synergism; $\frac{q^{mix}}{q_o} = 1$, there is no interaction between the species; $\frac{q^{mix}}{q_o} < 1$, the adsorption capacity gets suppressed due to the presence of other ion or is said to be showing antagonistic interaction of the two ions. The values obtained by $\frac{q^{mix}}{q_o}$ (Table 4) depicts that the power of adsorption of Fe_3O_4-SD decreases for single Cu(II) or Ni(II) when present in binary system than when present alone. As there exists a competition between the ions for getting adsorbed on the surface, antagonistic behavior is clearly indicated. Such a behavior in the bicomponent system may be seen due to different electronegativities and ionic potentials of the two species.

3.10. Regeneration and reusability of adsorbent

Regenerating of adsorbents helps in recovery of Cu(II) and Ni(II) ions along with the reuse of adsorbents. Desorption of Cu(II) and Ni(II) ions from Fe_3O_4-SD nanoparticles was tested using four different eluents (0.1 N H_2SO_4, 0.1 N HCl, 0.1 N HNO_3, and distilled water). Desorption ability of 0.1 N H_2SO_4 was found to be much better than that of others. Cu(II) ions had a greater tendency of getting desorbed into solution than Ni(II) ions for all the cases. On moving toward distilled water from 0.1 N H_2SO_4, the desorption efficiency dropped as 99.38, 87.3, 62.1, and 5.1% for Cu(II) and 97, 84.14, 61.45, and 2.3% for Ni(II) ions,

respectively, for the series of eluents. Reusability of the adsorbent was tested by subjecting it to the number of adsorption–desorption cycles. For this, Cu(II)- and Ni(II)-loaded adsorbent was dipped into 0.1 N H_2SO_4 and was agitated for the same time as taken for adsorption to reach equilibrium. The regenerated material was washed several times with distilled water to make its surface ready for another adsorption phase. It was deduced that Fe_3O_4-SD can be used up to four cycles with a decrement of only 10% adsorption efficiency.

4. Conclusion

The efficiency of magnetic nanoparticles prepared by co-precipitation of $FeCl_3 \cdot 6H_2O$ and $FeSO_4 \cdot 7H_2O$ along with sawdust in removing Cu(II) and Ni(II) ions from aqueous solutions has been investigated. A low dosage of 5 g/L has been found effective in simultaneous adsorption of Cu(II) and Ni(II) from the solutions. The pH 5 was found to be suitable and equilibrium was attained within 90 min of adsorbent–adsorbate contact. Better results were obtained for a dilute Cu(II) and Ni(II) concentration. Physisorption through complexation and ion exchange was seen occurring and the mechanism was thermodynamically proved to be spontaneous and favorable. For a wide range of concentration, system followed Langmuir isotherm. Competition for the sites existed between Cu(II) and Ni(II), thereby showing antagonistic nature. Such particles have economical feasibility and the power of removing metallic pollutants up to a greater extent. In addition to this, there was no release of Fe ions into the solutions; hence dissolution of some extra ions was not an issue. Thus, the data presented can help in designing treatment plants of Cu(II)- and Ni(II)-rich water and control of environmental pollution.

References

[1] A. Verma, O. Uzun, Y. Hu, Y. Hu, H.S. Han, N. Watson, S. Chen, D.J. Irvine, F. Stellacci, Surface-structure-regulated cell-membrane penetration by monolayer-protected nanoparticles, Nat. Mater. 7 (2008) 588–595.

[2] A.F. Ngomsik, A. Bee, M. Draye, G. Cote, V. Cabuil, Magnetic nano- and microparticles for metal removal and environmental applications: A review, C.R. Chim. 8 (2005) 963–970.

[3] L.S. Nair, C.T. Laurencin, Silver nanoparticles: Synthesis and therapeutic applications, J. Biomed. Nanotechnol. 3 (2007) 301–316.

[4] E. Weir, A. Lawlor, A. Whelan, F. Regan, The use of nanoparticles in anti-microbial materials and their characterization, Analyst 133 (2008) 835–845.

[5] V. Kandavelu, H. Kastien, K.R. Thampi, Photocatalytic degradation of isothiazolin-3-ones in water and emulsion paints containing nanocrystalline TiO_2 and ZnO catalysts, Appl. Catal., B 48 (2004) 101–111.

[6] S. Mann, Nanotechnology and Construction, Nanoforum Report, Institute of Nanotechnology, Stirling, 2006.

[7] C.M. Gonzalez, J. Hernandez, J.G. Parsons, J.L.G. Torresdey, A study of the removal of selenite and selenate from aqueous solutions using a magnetic iron/manganese oxide nanomaterial and ICP-MS, Microchem. J. 96 (2010) 324–329.

[8] D.S. Han, B. Batchelor, S.H. Park, A.A. Wahab, As(V) adsorption onto nanoporous titania adsorbents (NTAs): Effects of solution composition, J. Hazard. Mater. 229–230 (2012) 273–281.

[9] Y. Feng, J.L. Gong, G.M. Zeng, Q.Y. Niu, H.Y. Zhang, C.G. Niu, J.H. Deng, M. Yan, Adsorption of Cd(II) and Zn(II) from aqueous solutions using magnetic hydroxyapatite nanoparticles as adsorbents, Chem. Eng. J. 162 (2010) 487–494.

[10] A. Bhatnagar, E. Kumar, M. Sillanpää, Nitrate removal from water by nano-alumina: Characterization and sorption studies, Chem. Eng. J. 163 (2010) 317–323.

[11] P. Panneerselvam, N. Morad, K.A. Tan, Magnetic nanoparticle (Fe_3O_4) impregnated onto tea waste for the removal of nickel(II) from aqueous solution, J. Hazard. Mater. 186 (2011) 160–168.

[12] H. Ye, Q. Zhu, D. Du, Adsorptive removal of Cd(II) from aqueous solution using natural and modified rice husk, Bioresour. Technol. 101 (2010) 5175–5179.

[13] M. Rao, A.V. Parwate, A.G. Bhole, Removal of Cr^{6+} and Ni^{2+} from aqueous solution using bagasse and fly ash, Waste Manage. 22 (2002) 821–830.

[14] M. Jain, V.K. Garg, K. Kadirvelu, Chromium(VI) removal from aqueous system using *Helianthus annuus* (sunflower) stem waste, J. Hazard. Mater. 162 (2009) 365–372.

[15] M. Thirumavalavan, Y.L. Lai, J.F. Lee, Fourier transform infrared spectroscopic analysis of fruit peels before and after the adsorption of heavy metal ions from aqueous solution, J. Chem. Eng. Data 56 (2011) 2249–2255.

[16] K.K. Panday, G. Prasad, V.N. Singh, Copper(II) removal from aqueous solutions by fly ash, Water Res. 19 (1985) 869–873.

[17] V.K. Gupta, A. Rastogi, M.K. Dwivedi, D. Mohan, Process development for the removal of zinc and cadmium from wastewater using slag—A blast furnace waste material, Sep. Sci. Technol. 32 (1997) 2883–2912.

[18] M. Kapur, M.K. Mondal, Mass transfer and related phenomena for Cr(VI) adsorption from aqueous solutions onto *Mangifera indica* sawdust, Chem. Eng. J. 218 (2013) 138–146.

[19] S. Chamarthy, C.W. Seo, W.E. Marshall, Adsorption of selected toxic metals by modified peanut shells, J. Chem. Technol. Biotechnol. 76 (2001) 593–597.

[20] M.K. Mondal, Removal of Pb(II) ions from aqueous solution using activated tea waste: Adsorption on a fixed-bed column, J. Environ. Manage. 90 (2009) 3266–3271.

[21] V.K. Gupta, A. Nayak, Cadmium removal and recovery from aqueous solutions by novel adsorbents prepared from orange peel and Fe_2O_3 nanoparticles, Chem. Eng. J. 180 (2012) 81–90.

[22] APHA, Standard Methods for Examination of Water and Wastewater, 14th ed., American Public Health Association, Washington, DC, 1975.

[23] Y. Gao, R. Wahi, A.T. Kan, J.C. Falkner, V.L. Colvin, M.B. Tomson, Adsorption of cadmium on anatase nanoparticles effect of crystal size and pH, Langmuir 20 (2004) 9585–9593.

[24] A.K. Gupta, S. Wells, Surface-modified superparamagnetic nanoparticles for drug delivery: Preparation, characterization, and cytotoxicity studies, IEEE Trans. Nanobiosci. 3 (2004) 66–73.

[25] B. Stuart, Infrared Spectroscopy: Fundamentals and Applications, J. Wiley, Chichester, West Sussex, England, Hoboken, NJ, 2004.

[26] J.C. Zheng, H.M. Feng, M.H.W. Lam, P.K.S. Lam, Y.W. Ding, H.Q. Yu, Removal of Cu(II) in aqueous media by biosorption using water hyacinth roots as a biosorbent material, J. Hazard Mater. 171 (2009) 780–785.

[27] M.H. Liao, D.H. Chen, Preparation and characterization of a novel magnetic nano-adsorbent, J. Mater. Chem. 12 (2002) 3654–3659.

[28] Y. Chi, W. Geng, L. Zhao, X. Yan, Q. Yuan, N. Li, X. Li, Comprehensive study of mesoporous carbon functionalized with carboxylate groups and magnetic nanoparticles as a promising adsorbent, J. Colloid Interface Sci. 369 (2012) 366–372.

[29] K.V.P.M. Shafi, A. Gedanken, R. Prozorov, J. Balogh, Sonochemical preparation and size-dependent properties of nanostructured $CoFe_2O_4$ particles, Chem. Mater. 10 (1998) 3445–3450.

[30] G.D. Sheng, J.X. Li, D.D. Shao, J. Hu, C.L. Chen, Y.X. Chen, X.K. Wang, Adsorption of copper(II) on multi-walled carbon nanotubes in the absence and presence of humic or fulvic acids, J. Hazard. Mater. 178 (2010) 333–340.

[31] G. Zhao, H. Zhang, Q. Fan, X. Ren, J. Li, Y. Chen, X. Wang, Sorption of copper(II) onto super-adsorbent of bentonite–polyacrylamide composites, J. Hazard. Mater. 173 (2010) 661–668.

[32] S. Lagergren, Zur theorie der sogenannten adsorption gelöster stoffe (About the theory of so-called adsorption of soluble substances), K. Svenska Vetenskapsakad. Handl. 24 (1898) 1–39.

[33] G. McKay, Y.S. Ho, Pseudo-second order model for sorption processes, Process Biochem. 34 (1999) 451–465.

[34] C.W. Cheung, J.F. Porter, G. Mckay, Sorption kinetics for the removal of copper and zinc from effluents using bone char, Sep. Purif. Technol. 19 (2000) 55–64.

[35] W.J. Weber, J.C. Morris, Equilibria and capacities for adsorption on carbon, J. Sanitary Eng. Div. 90 (1964) 79–107.

[36] Y. Seki, K. Yurdakoç, Adsorption of promethazine hydrochloride with KSF montmorillonite, Adsorption 12 (2006) 89–100.

[37] C.J. Radke, J.M. Prausnitz, Thermodynamics of multi-solute adsorption from dilute liquid solutions, AlChE J. 18 (1972) 761–768.